IOPscience iopscience.iop.org

Home Search Collections Journals About Contact us My IOPscience

Carbon-induced extreme ultraviolet reflectance loss characterized using visible-light ellipsometry

This article has been downloaded from IOPscience. Please scroll down to see the full text article.

2011 Meas. Sci. Technol. 22 105705

(http://iopscience.iop.org/0957-0233/22/10/105705)

View the table of contents for this issue, or go to the journal homepage for more

Download details:
IP Address: 130.89.112.86
The article was downloaded on 05/06/2012 at 13:07

Please note that terms and conditions apply.

Meas. Sci. Technol. **22** (2011) 105705 (8pp) doi:10.1088/0957-0233/22/10/105705

Carbon-induced extreme ultraviolet reflectance loss characterized using visible-light ellipsometry

Juequan Chen[1], Eric Louis[1], Herbert Wormeester[2], Rob Harmsen[1], Robbert van de Kruijs[1], Chris J Lee[2], Willem van Schaik[3] and Fred Bijkerk[1,2]

[1] FOM-Institute for Plasma Physics Rijnhuizen, Edisonbaan 14, 3439 MN Nieuwegein, The Netherlands
[2] MESA+ Institute for Nanotechnology, University of Twente, 7500 AE Enschede, The Netherlands
[3] ASML BV, De Run 1110, 5503 LA Veldhoven, The Netherlands

E-mail: J.Chen@rijnhuizen.nl

Received 21 February 2011, in final form 22 July 2011
Published 2 September 2011
Online at stacks.iop.org/MST/22/105705

Abstract
Carbon deposition on extreme ultraviolet (EUV) optics was observed due to photon-induced dissociation of hydrocarbons in a EUV lithography environment. The reflectance loss of the multilayer mirror is determined by the carbon layer thickness and density. To study the influence of various forms of carbon, EUV-induced carbon, hot filament and e-beam evaporated carbon were deposited on EUV multilayer mirrors. Spectroscopic ellipsometry was used to determine the carbon layer thickness and the optical constants ranging from ultraviolet to near infrared. The carbon density (and thus reflectance loss) was determined from the optical constants using both Bruggeman's effective medium approximation and the Clausius–Mosotti equation. Both approaches result in a similar EUV reflectance loss, with an accuracy of about 4%. The application of this process to ultrathin carbon films is further discussed.

Keywords: carbon deposition, EUV reflectance loss, ellipsometry

(Some figures in this article are in colour only in the electronic version)

1. Introduction

Extreme ultraviolet lithography (EUVL) is a next-generation lithographic technique that uses 13.5 nm or extreme UV radiation. The reflectance of each lithography optical element at this EUV wavelength is one of the most important parameters that influence the throughput of the lithographic equipment. Carbon contamination is one of the main surface contamination processes that reduces the reflectance of the Mo/Si multilayer mirrors (MLMs) used [1]. One of the challenges in developing EUVL is the development of effective and rapid cleaning techniques.

Different types of carbon contamination under photon radiation, i.e. graphite- or polymer-like, have been observed [1–3]. The specific type of carbon contamination expected in the EUVL environment can be influenced by several factors, including residual background gas, radiation flux, geometry of illumination and the temperature of the optics. Determining the type of carbon contamination is important both for the cleaning procedure and the induced reflectance loss.

Calculations show that a 2 nm thick layer of carbon in the form of graphite (density 2.25 g cm^{-3}) would reduce the reflectance of an MLM by 5%. On the other hand, as an example, as described by Hollenshead and Klebanoff [1], the projection optics of EUVL equipment should not lose more than 1.6% reflectance per optic. This means we have to deal with ultrathin carbon films of less than 2 nm in EUVL applications.

Due to lack of space, using a reflectometer in the EUV lithography environment to measure the reflectance loss directly is very difficult. Therefore, an alternative technique for monitoring the contamination is required to enable *in situ*

 © 2011 IOP Publishing Ltd Printed in the UK & the USA

reflectance loss estimation. To estimate the reflectance loss of each multilayer mirror, both the carbon layer thickness and density are needed. Spectroscopic ellipsometry (SE) is one of the best candidates for *in situ* monitoring of carbon deposition [4]. SE has a detection limit of about 0.1 nm.

The carbon densities are usually determined using electron energy loss spectroscopy (EELS) [5, 6], a combination of ellipsometry with nuclear reaction analysis (NRA) [7, 8], proton-enhanced cross-section scattering (PES) [9], or Rutherford backscattering (RBS) [10]. All of these techniques require substantial amounts of space within the vacuum chamber, making them undesirable for EUVL.

In this paper, we estimate the carbon density from the optical constants in the wavelength range of ultraviolet (UV) to near infrared (NIR) using two approaches: Bruggeman's effective medium approximation (BEMA) and the Clausius–Mosotti (CM) equation. We show the applicability of SE by investigating the reflectance loss of MLMs after the deposition of different kinds of carbon films. The EUV reflectance loss was estimated from the carbon density and thickness, as derived from SE measurements.

These estimates were compared with the measured EUV reflectance loss. Good agreement was obtained between the measured and the estimated reflectance loss. This work establishes SE as an excellent technique for *in situ* monitoring carbon contamination of MLMs in EUVL. The applicability for ultrathin carbon films, in which case the individual determination of the refractive index and the thickness is very difficult, will be discussed.

2. Methodology

Briefly, the MLMs investigated consist of 50 bi-layers of Mo and Si, each about 7 nm thick, deposited on the (001) surface of a Si wafer. Each MLM has a capping layer terminating the structure. A complete description of a typical MLM structure and its properties can be found elsewhere [11].

Three types of carbon layers have been investigated. The first type, called 'EUV induced C', was grown by exposing the MLM to EUV radiation in the presence of residual hydrocarbon gases. Four different thicknesses were obtained by varying the number of pulses of EUV light. The second type of carbon layer, referred to as the 'hot filament C', was deposited by evaporation from a graphite filament. The third type of carbon layer was deposited using physical vapor deposition (PVD) after e-beam evaporation of a graphite target. This layer is referred to as 'PVD C'.

The optical characterization of the EUV-induced carbon and hot filament carbon was done *ex situ* using variable angle SE (Woollam, VASE, spectral range 245–1689 nm). The PVD carbon deposition was monitored with *in situ* ellipsometry (Woollam, M2000, incidence angle of 55° with respect to the surface normal). Standard procedures for data analysis and deducing the thickness and optical constants of the carbon films were used [12, 13].

To establish the carbon density, a set of carbon films was deposited on a silicon wafer and analyzed with grazing incidence x-ray reflectivity (GIXR) [14]. An *ex situ* reflectometer, based on $\lambda = 0.154$ nm (Cu-K_α), was used. The critical angle for total external reflection was used to determine the total electron density, which provides the mass density. Furthermore, the thickness of the top carbon layer is determined by fitting the period of the interference pattern.

The EUV reflectance for these carbon-covered MLMs was measured with a reflectometer at the radiometry laboratory of the Physikalisch-Technische Bundesanstalt (PTB) at the BESSY II electron storage ring. The estimated reflectance of a carbon-covered MLM was calculated using the IMD program [15].

3. Principle of EUV reflectance loss

The refractive index (and thus the dielectric function) at EUV wavelength and soft x-rays can be described by the authors of [16]:

$$n(\lambda) = 1 - \delta + \mathrm{i}\beta, \qquad (1)$$

where

$$\delta = \frac{n_a r_e \lambda^2}{2\pi} f_1^0(\lambda) \quad \text{and} \quad \beta = \frac{n_a r_e \lambda^2}{2\pi} f_2^0(\lambda),$$

where n_a is the atomic density, r_e is the classical electron radius and λ is the radiation wavelength. $f_1^0(\lambda)$ and $f_2^0(\lambda)$ are the atomic scattering factors as a function of wavelength. The atomic scattering factors of carbon and hydrogen from [16] were used in our calculations.

Equation (1) shows that the refractive index for EUV and soft x-rays of different kinds of carbon films is determined only by the atomic density. In other words, the carbon atoms in solids react to the incident EUV radiation as if they are isolated atoms. The specific carbon bonds present (i.e. sp^1, sp^2 and sp^3) or the band structure of the different kinds of carbon films does not affect the absorption process of the incident radiation. Furthermore, the accuracy of equation (1) has been verified for polymer films [17].

The refractive indices at the EUV wavelength of 13.5 nm for diamond (density 3.51 g cm^{-3}), graphite (density 2.25 g cm^{-3}) and polyethylene (density 0.90 g cm^{-3}) were computed with IMD. The geometry considered was a carbon layer on top of an MLM at an angle of incidence of 1.5° with respect to the surface normal.

The relative EUV reflectance loss, $\Delta R/R$, is

$$\Delta R/R = \frac{R - R_0}{R_0} \times 100\%, \qquad (2)$$

where R_0 is the original EUV reflectance of an MLM and R is the reflectance upon carbon deposition. Figure 1(*a*) shows the calculated relative EUV reflectance loss, $\Delta R/R$, as a function of carbon layer thickness for the three types of carbon films. The general trend is that the EUV reflectance decreases with increasing carbon layer thickness. The influence of the carbon density on the EUV reflectance loss is strong. For instance, the relative reflectance loss due to a 2 nm thick layer of diamond (7.6%) is 3.8 times higher than that of the same thickness of polyethylene. The oscillations of the curves are due to the interference between the carbon surface and the interface between the carbon layer and the MLM.

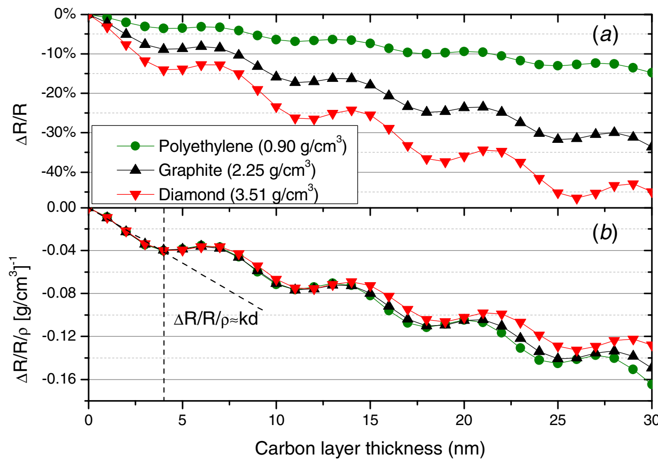

Figure 1. Calculated relative EUV reflectance loss from an MLM (*a*) as a function of the carbon layer thickness for different carbon densities corresponding to different types of carbon films. (*b*) The reflectance loss normalized by the carbon density.

The oscillation amplitude is determined by the optical contrast between the carbon layer and the substrate underneath.

Figure 1(*b*) shows the relative reflectance loss normalized by the carbon density. The different types of carbon films can be seen to give nearly the same reflectance loss level per unit density. This shows that the reflectance attenuation scales with the density and multiple interferences between the surface and interface have only a minor effect. Especially, for a carbon layer less than 4 nm thick, corresponding to a practical case in EUVL applications, the relative reflectance loss curve can be simplified to a linear relationship as

$$\Delta R/R \approx k\rho d, \tag{3}$$

where k is a constant equal to the slope as indicated in figure 1(*b*), ρ is the average mass density and d is the carbon layer thickness. The suitability of the approximation depends on the substrate. As an example, it fails for a substrate of bulk Mo and carbon layers in the same thickness range because the optical contrast leads to much stronger interference effects. For ultrathin carbon films, equation (3) will be used to determine the reflectance loss, based on estimates of ρd from ellipsometer measurements and effective medium approximation (discussed below).

4. Estimating the carbon density from the optical constants

To calculate the attenuation of the EUV reflectance upon carbon contamination on an MLM, the dielectric function of the carbon layer in the EUV wavelength range is required. A simple extrapolation of the dielectric function from the accessible region of ellipsometry is not feasible because of the substantial amount of absorption between 10 and 20 eV [6, 18, 19]. However, in our case, it is only necessary to know the density of carbon to calculate the change in EUV optical properties.

Estimates of carbon density, based on ellipsometric data, are complicated by the different bond structures of the different types of carbon layers. The sp^3 bonds in diamond result in a large band gap between the bonding and antibonding σ bonds, leading to absorption in the UV range. The introduction of sp^2 bonds, as found in graphite-like carbon, introduces the bonding and antibonding π bands close to the Fermi energy. This results in a higher refractive index in the visible range. However, the carbon density decreases for this higher refractive material. Table 1 lists refractive indices at a wavelength of 600 nm, and carbon densities for several carbon species. These examples show that it is difficult to estimate the refractive index in the EUV region from refractive index data in the UV-NIR region.

Table 1. The refractive index and extinction coefficient at 600 nm and the densities for four different kinds of carbon films.

Carbon type	n	k	Density (g cm^{-3})	Reference
Diamond	2.42	0	3.515	[26, 27]
HOPG[a]	3.19	1.80	2.266	[27, 28]
50/50-C[b]	2.83	0.85	2.891	[26, 27]
Polyethylene	1.48	0	0.92	[29, 5]

[a] The refractive index of HOPG was measured in our experiments.
[b] 50/50-C is a defined effective medium with 50% diamond and 50% HOPG.

The refractive index of carbon films, as well as their densities, has been investigated by several groups [5–10, 20–23]. These carbon films are diamond-like (sp^3 bond), graphite-like (sp^2 bond) or polymer-like (H-content). The refractive indices of these films were all measured by ellipsometry. The accuracy of the carbon densities reported is about 10%.

These literature results, as well as our own measurements, are shown in figures 2(*a*), (*b*) and table 1. The value of the refractive index at a wavelength of 600 nm was chosen because it is the most common wavelength for ellipsometry or reflectometry in the literature. The properties of bulk diamond, highly ordered pyrolytic graphite (HOPG) and polyethylene, $(C_2H_4)_n$, are also depicted. From figure 2, it is observed that all the experimental values lie within the triangle defined by diamond, HOPG and $(C_2H_4)_n$. The location of a particular film within this triangle characterizes it as diamond-like, graphite-like or polymer-like, as indicated in the figure. Moreover, a trend relating carbon density to the refractive index is observed.

Four main methods have been proposed and used to estimate the carbon density from the optical properties in the UV-NIR range. In the first method, developed by the authors of [24], a linear relationship between the square of the refractive index (n^2) and the density ($n^2(E) - 1 \propto \rho$ for $E \ll E_g$, the energy gap) was found for amorphous carbon which means that the density can be estimated based on the refractive index. However, this method is only applicable for carbon films with an extinction coefficient equal to zero for the photon energy used, or in other words, where $E \ll E_g$. For graphite-like carbon (e.g. our hot filament carbon and PVD carbon), this is not the case. Therefore, we do not use this method in this paper. In the second method, used in [25], the maximum value of the imaginary part of the dielectric function,

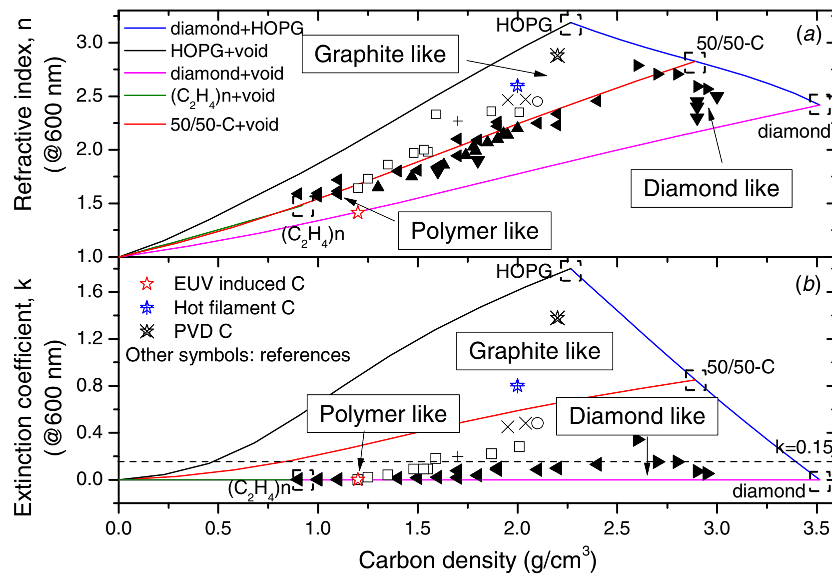

Figure 2. Calculated refractive index (*a*) and extinction coefficient (*b*) for a wavelength of 600 nm as a function of carbon density based on BEMA. The five curves correspond to the compositions of 'diamond+HOPG', 'HOPG+void', 'diamond+void', '$(C_2H_4)_n$+void' and '50/50-C+void'. The experimental data in the references are also plotted with symbols as a comparison (▲ [7], ▼ [21], ◄ [9], ► [6], □ [8], ○ [10], × [20, 23], + [22]). The extinction coefficient $k = 0.15$ is a defined boundary between diamond-like (or polymer-like) and graphite-like carbon.

$e2_{max}$ was used as a measure of the film density. However, $e2_{max}$ only provides qualitative variations of the density and is not adequately accurate. The other two methods are based on BEMA and the CM equation. Below, we use these two methods to estimate the density of carbon films on MLMs.

4.1. Effective medium approximation

The BEMA is broadly applied to estimate the relationship between the density and the refractive index for a variety of semiconductor and dielectric materials [30–32, 25]. In this case, the carbon film is considered to be a porous film, consisting of voids and carbon. The carbon can be present as diamond, HOPG or $(C_2H_4)_n$, reflecting the various carbon bonding geometries. We also define a synthetic material, consisting of 50% diamond and 50% HOPG (50/50-C), i.e. a combination of sp^3 and sp^2 bonding. The effective dielectric function, ε_{eff}, is calculated from the BEMA equation [13]

$$0 = f_v \frac{\varepsilon_v - \varepsilon_{eff}}{\varepsilon_v + 2\varepsilon_{eff}} + f_C \frac{\varepsilon_C - \varepsilon_{eff}}{\varepsilon_C + 2\varepsilon_{eff}}, \quad (4)$$

where f_v and f_C denote the volume fraction of void and carbon ($f_v + f_C = 1$) while ε_v and ε_C are their respective dielectric functions. The complex refractive index of the film equals $\sqrt{\varepsilon_{eff}}$. The density is f_C times the carbon density corresponding to graphite, diamond or polyethylene.

Figure 2 shows the calculated relationship between the complex refractive index (i.e. the real part n and the imaginary part k) and density, based on equation (4). Five compositions are displayed: 'diamond+HOPG', 'HOPG+void', 'diamond+void', '$(C_2H_4)_n$+void' and '50/50-C+void'. The slope of the curve 'HOPG+void' is much steeper than that of the curve 'diamond+void' for both the real and imaginary parts of the refractive index. Note that the results of '$(C_2H_4)_n$+void' and '50/50-C+void' are very similar for the real part of the refractive index. However, the extinction coefficient shows very different behavior, with the '$(C_2H_4)_n$+void' curve close to the 'diamond+void' as both are transparent at the wavelength of 600 nm.

The experimental refractive index data for carbon films fall roughly into two categories, diamond-like and graphite-like, as can be seen in figure 2(*a*). They tend to cluster around the '50/50-C+void' that separates the two regions. However, figure 2(*b*) shows that the extinction coefficient for most of the experimental values is close to $k = 0$ instead of the '50/50-C+void' curve. This can be explained by the connectivity of the non-void regions. The absorption of HOPG is dominated by conductive electrons; thus, it is instructive to examine the BEMA, as applied to a metal-dielectric composite. The conductivity of the effective medium is zero if the relative volume fraction of the metal constituent is less than $1/D$, where D is the dimension [33]. This is the so-called percolation threshold. For a three-dimensional sample consisting of spherical grains, the percolation threshold is 1/3, while for two-dimensional samples it is 1/2. For a carbon film, the extinction coefficient at 600 nm results from free electron absorption and absorption due to π electrons in the sp^2 bonds. An example is the extinction coefficient of graphite as shown in [6]. This means that for carbon films with sp^2 bonded carbon volume less than the percolation threshold (1/3–1/2), the absorption due to free electrons vanishes. This results in the decrease of the extinction coefficients as shown in figure 2(*b*) as a contrast to figure 2(*a*).

For carbon films whose refractive index and density are very close to the curve '50/50-C+void', their extinction coefficients are close to $k = 0.15$ at 600 nm. Generally, we refer to this kind of carbon as amorphous carbon. Based on this, we define a boundary at $k = 0.15$ (shown in figure 2(*b*))

Table 2. Static polarizability of different types of carbon and hydrocarbons.

Carbon type	Static polarizability (10^{-24} cm^3)	Reference
Diamond	0.815	[36]
Graphite	1.61[a]	[35]
Graphite	1.76	[37]
Graphite	1.265	[38]
C_2H_2	3.33	[37]
C_2H_4	4.252	[37]
C_2H_6	4.47	[37]

[a] Averaged polarizability is used.

to separate diamond-like and polymer-like carbon ($k < 0.15$) from graphite-like carbon ($k \geqslant 0.15$).

Figure 2 shows that the BEMA can be used to establish a relation between the complex refractive index and the carbon density. It also means that the carbon density can be estimated from the refractive index and extinction coefficient. The density was estimated from the BEMA using the value of the refractive index and extinction coefficient at 600 nm because this wavelength provides the minimum uncertainty range of carbon density. For a given refractive index (also extinction coefficient), the range of possible densities lies on the line of the constant refractive index (also extinction coefficient) that begins at the intersection with the black 'HOPG + void' curve and terminates at either the purple 'diamond + void' (only for refractive index) or blue 'diamond + HOPG' curves. In order to reduce the range of the density determined by the refractive index, a carbon film is defined as diamond-like (or polymer-like) if its extinction coefficient is less than 0.15, and graphite-like if it is greater than 0.15. The two film types have their boundary along the '50/50-C + void' curve. Once the type of film is determined, the upper (lower) density limit for graphite-like (diamond-like or polymer-like) films is given by the intersection between the line of constant refractive index and the orange '50/50-C + void curve'.

4.2. The CM equation

The CM formula has been used by several authors to relate the density and the dielectric function [34, 31, 32, 35]. The CM equation is

$$\alpha(0) = \frac{3}{4\pi N}\left(\frac{e1(0)-1}{e1(0)+2}\right), \qquad (5)$$

where $\alpha(0)$ is the static polarizability (i.e. at zero photon energy) and $e1(0)$ is the real part of dielectric function at zero photon energy, and the medium is made up of N atoms (or ions) per unit volume.

The static polarizability for carbon is different for its various forms, graphite, diamond and hydrocarbon polymers (see table 2). Hydrocarbon molecules C_2H_2, C_2H_4 and C_2H_6 are representative of the main constituents in polymer-like carbon films. For graphite, the polarizability is anisotropic [35], so the average polarizability is used in our calculations. Figure 3 shows the static dielectric function $e1(0)$ as a function of the carbon density according to the CM equation (5).

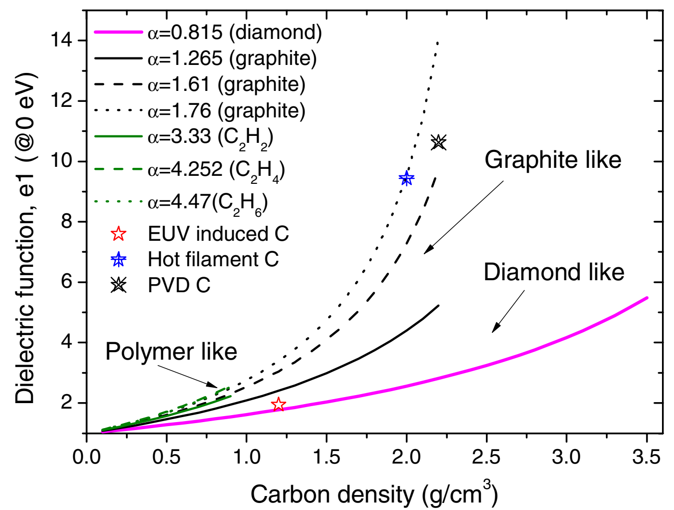

Figure 3. Calculated static dielectric function, $e1$ (@0 eV) as a function of carbon density, according to the CM equation. The seven curves correspond to the static polarizability values of diamond, graphite and polymers listed in table 2. Our experimental data for EUV-induced C, hot filament C and PVD C are also plotted with blue stars.

Diamond-like carbon lies in the region between $\alpha(0) = 0.815$ and 1.265, and graphite-like carbon lies in the region between $\alpha(0) = 1.265$ and 1.76.

The static dielectric function $e1(0)$ cannot be measured directly with ellipsometry; however, it can be estimated by extrapolating from the UV-NIR, based on the parameterization of the dielectric functions of different types of carbon films [6]. The extrapolated values for the measured carbon films are shown in figure 3.

As the estimation of density based on the BEMA, a similar procedure was used for the method based on the CM equation. The extrapolated dielectric function, $e1$, at photon energy of zero, $e1(0)$, was obtained by extrapolating the dielectric function in the NIR-UV. The boundary $k = 0.15$ at the wavelength of 600 nm was used to determine the carbon type. Taking into account the range of the reported values of polarizabilities in the literature, as shown in table 2, a density range was calculated based on equation (5). As shown in figure 3, the estimated upper and lower limits for diamond-like carbon films are determined by the curve of $\alpha(0) = 0.815$ (diamond) and 1.265 (graphite). While for graphite-like carbon films, the limits are determined by the density curves with limiting values given by $\alpha(0) = 1.265$–1.76 (graphite). The HOPG density of 2.266 g cm^{-3} was applied as the upper limit of the density of graphite-like carbon. For those carbon films with $e1(0)$ close to 2, corresponding to polymer-like films, we applied the maximum limits determined by the curve of $\alpha(0) = 0.815$ (diamond) and 4.252 (C_2H_4).

5. Estimation of EUV reflectance loss

As described in section 3, to estimate the EUV reflectance loss of an MLM due to carbon deposition, both the carbon layer thickness and density are required. The BEMA and CM equation were used to estimate the carbon density. As

Table 3. Estimation of carbon density according to the refractive index or the dielectric function based on the BEMA and the CM equation. The upper and lower limits are listed. The measured density by GIXR is also listed as a comparison.

Carbon type	n@600 nm	Density$^+$ (g cm^{-3})	Density$^-$ (g cm^{-3})	$e1$@0 eV	Density$^+$ (g cm^{-3})	Density$^-$ (g cm^{-3})	Density (g cm^{-3})
Method	Measured	BEMA	BEMA	Extrapolated	CM	CM	GIXR
EUV C	1.41	1.17	0.79	1.95	1.40	0.63	1.2 ± 0.2
Hot C	2.60	2.53	1.68	9.44	2.266[a]	1.99	2.0 ± 0.1
PVD C	2.88	2.54[b]	1.95	10.63	2.266[a]	2.06	2.2 ± 0.2

[a] The density of HOPG is applied as the upper limit of graphite-like carbon.
[b] This limit is based on k (blue curve in figure 2(*b*)) because it is smaller than that based on n.

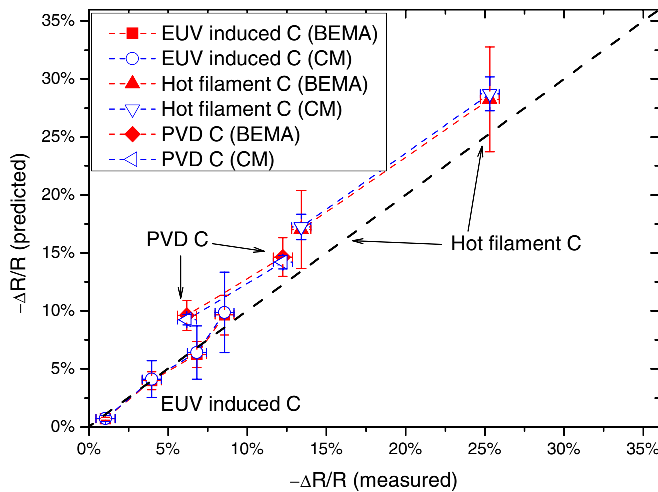

Figure 4. Comparison of relative EUV reflectance losses between the measured and estimated values based on BEMA and the CM equation with different carbon layer thicknesses including hot filament carbon, EUV-induced carbon and PVD carbon.

a comparison, the EUV reflectance was measured with a reflectometer and the relative reflectance loss was calculated based on equation (2).

Table 3 shows the range of estimated carbon densities calculated from the BEMA and the CM equation. The density, as measured by GIXR, is also listed as a comparison. There is good agreement between the three measurements.

Figure 4 shows the comparison of EUV reflectance loss measured and the estimated reflectance loss based on the densities derived from the BEMA and the CM equation for the three kinds of carbon films. The uncertainty of the measured reflectance loss was 0.6%, based on the absolute reflectance measurement error of 0.2%. On the other hand, the uncertainty of the estimated reflectance loss depends on the carbon type and the approach applied. In addition, for both approaches, the uncertainty range increases with increasing thickness.

First of all, the estimated reflectance losses of the four different EUV carbon films as calculated with both approaches agree well with the measured reflectance losses. For the hot filament carbon films, the BEMA estimated reflectance losses agree to within uncertainties with the measured reflectance losses, while the values calculated from the CM equation are 4% higher than the measured value. However, the BEMA estimated uncertainty is three times larger than that of the CM equation.

For the PVD carbon films, the estimated reflectance losses based on both approaches were about 4% higher than the measured values. Overall, for both the hot filament and PVD carbon, the estimated reflectance losses are all about 4% higher than the measured values. We believe that the main reason is the overestimation of the optical constants calculated from equation (1) for graphite-like carbon. On the other hand, only for polymer films, optical constants for the EUV wavelength range calculated from equation (1) have been confirmed experimentally [17].

As shown in figure 4, both the BEMA and the CM equation can be used to estimate the reflectance loss due to carbon deposition with a maximum systematic offset of 4% in the loss range of up to ∼30%. In addition, for EUV-induced carbon, the BEMA estimated reflectance loss agrees better with the experimental data. Furthermore, the complex refractive index at 600 nm can be obtained with ellipsometry directly for the BEMA. On the other hand, for the CM equation, the dielectric function at zero photon energy must be obtained through extrapolation. In addition, the polarizability limits used in the CM equation were obtained from literature values from unmixed samples, and it is unclear if these represent the full range of possible polarizability values for mixed samples. Overall, the BEMA works slightly better and appears more reliable than the CM equation for the estimation of the reflectance loss by determining the carbon density.

6. Application for ultrathin carbon films

For ultrathin films with a thickness of a few nanometers, it is very difficult to determine the refractive index and the thickness independently using SE. This is because, in the thin film limit, thickness and refractive index become correlated and only the product of the refractive index and thickness (i.e. nd) can be determined. For the BEMA method, figure 2(*a*) implies that a good relationship between nd and the product of the density and thickness (i.e. ρd) exists. The product of density and thickness is actually the amount of carbon per surface area, the critical factor for the EUV reflectance loss as we observed that $\Delta R/R \approx k\rho d$ (see equation (3)).

In order to reduce the estimated uncertainty range of ρd, we need to determine if a carbon film is graphite-like or diamond-like (also polymer-like). To achieve this, the change of the two ellipsometric angles (i.e. Ψ and Δ) as carbon is deposited has to be used. Figure 5 shows the trajectory of Ψ

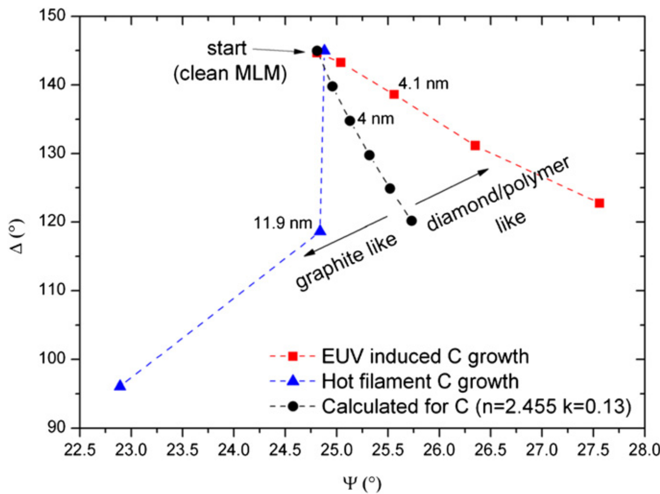

Figure 5. The trajectory of the ellipsometric angles, Ψ and Δ, at a wavelength of 600 nm, when a carbon layer is deposited on a multilayer mirror. The red squares and blue triangles correspond to the deposition of EUV-induced carbon and hot filament carbon, respectively. Another trajectory for carbon deposition with a complex refractive index of 2.455 + 0.13i was calculated and plotted as a rough boundary between graphite-like and diamond-like (also polymer-like carbon).

and Δ for a wavelength of 600 nm and an angle of incidence of 70° with respect to the surface normal. Each point is from a different MLM that has had a thicker layer of carbon deposited on it. As shown in figure 5, EUV-induced carbon and hot filament carbon display very different trajectories. This is because EUV-induced carbon is polymer-like while hot filament carbon is graphite-like. In addition, a calculated trajectory for a carbon film with a complex refractive index of 2.455 + 0.13i [9] is shown as a rough boundary between graphite-like and diamond-like (also polymer-like) (as shown in figure 2). This example shows that the trajectory of the two ellipsometry angles can be used to determine the type of carbon film, which in turn allows the density and reflectance loss of the carbon film to be accurately estimated.

7. Conclusion

The EUV reflectance loss of a multilayer mirror due to carbon deposition is mainly determined by the carbon layer thickness and the type of carbon deposited since the latter causes changes in refractive index (or dielectric function). In the EUV wavelength range, the refractive index of a carbon film is mainly determined by its atomic density. In this paper, SE has been used to determine the thickness and the refractive index for EUV-induced carbon, hot filament carbon and PVD carbon by e-beam evaporation on top of multilayer mirrors.

In order to estimate the carbon density from the refractive index in the wavelength range from ultraviolet to near infrared, two different approaches were analyzed. The first approach was based on BEMA. We observed that the experimental carbon densities as well as their refractive indices published are well described by the BEMA.

The second approach was based on the CM equation, which was used to derive the density of carbon films from an extrapolated dielectric function.

The EUV reflectance losses due to carbon depositions were measured with a reflectometer and compared to the estimated losses, based on the two approaches. Good agreement was obtained, with error estimates being at most 4% in the reflectance loss range from 0% up to ∼30%. This means that we could estimate the EUV reflectance loss accurately using SE.

For ultrathin carbon films with a thickness of a few nanometers, we can determine the type of carbon by the trajectory of the two ellipsometry angles. Since determination of the refractive index and thickness independently is very difficult, we determined the product of the refractive index and thickness (i.e. nd). Furthermore, using the BEMA, we show that the product of the density and thickness (i.e. ρd) can be estimated from the parameter nd. Finally, we show that a simplified relationship between the reflectance loss and the product of density and thickness (i.e. $\Delta R/R \approx k\rho d$) can be used to estimate the reflectance loss due to carbon deposition.

Acknowledgments

This research was carried out under the project number MC3.06245 in the framework of the Research Program of the Materials innovation institute M2i (www.m2i.nl). Also this work is part of the research programme 'Controlling photon and plasma induced processes at EUV optical surfaces (CP3E)' of the 'Stichting voor Fundamenteel Onderzoek der Materie (FOM)', which is financially supported by the 'Nederlandse Organisatie voor Wetenschappelijk Onderzoek (NWO)'. The CP3E programme is co-financed by Carl Zeiss SMT and ASML. We acknowledge Jan-Willem Weber, T A R Hansen and M C M van de Sanden at the University of Technology Eindhoven, Thomas Wagner at LOT-Oriel GmbH & Co. KG for assistance in the ellipsometry data analysis; Eddie van Hattum at FOM-Rijnhuizen for the help with EUV reflectance measurements; Saskia Bruijn at FOM-Rijnhuizen for the help with GIXR measurements and analysis; Roel Moors and Maarten van Kampen at ASML for the preparation of the EUV carbon samples; and Jan Verhoeven at Leiden University for the help with the e-beam deposition.

References

[1] Hollenshead J and Klebanoff L 2006 Modeling radiation-induced carbon contamination of extreme ultraviolet optics *J. Vac. Sci. Technol.* B **24** 64–82

[2] Boller K-J, Haelbich R-P, Hogrefe H, Jark W and Kunz C 1983 Investigation of carbon contamination of mirror surfaces exposed to synchrotron radiation *Nucl. Instrum. Methods Phys. Res.* **208** 273–9

[3] Chen J Q, Lee C J, Louis E, Bijkerk F, Kunze R, Schmidt H, Schneider D and Moors R 2009 Characterization of EUV induced carbon films using laser-generated surface acoustic waves *Diam. Relat. Mater.* **18** 768–71

[4] Chen J Q *et al* 2009 Detection and characterization of carbon contamination on EUV multilayer mirrors *Opt. Express* **17** 16969–79

[5] Robertson J 2002 Diamond-like amorphous carbon *Mater. Sci. Eng.* R **37** 129–281

[6] Waidmann S, Knupfer M, Fink J, Kleinsorge B and Robertson J 2001 Electronic structure studies of undoped and nitrogen-doped tetrahedral amorphous carbon using high-resolution electron energy-loss spectroscopy *J. Appl. Phys.* **89** 3783–92

[7] Koidl P, Wild C, Dischler B, Wagner J and Ramsteiner M 1989 Plasma deposition, properties and structure of amorphous hydrogenated carbon films *Mater. Sci. Forum* **52-53** 41–70

[8] Godet C, Conway N M J, Bouree J E, Bouamra K, Grosman A and Ortega C 2002 Structural and electronic properties of electron cyclotron resonance plasma deposited hydrogenated amorphous carbon and carbon nitride films *J. Appl. Phys.* **91** 4154–62

[9] Schwarz-Selinger T, von Keudell A and Jacob W 1999 Plasma chemical vapor deposition of hydrocarbon films: the influence of hydrocarbon source gas on the film properties *J. Appl. Phys.* **86** 3988–96

[10] Singh S V, Creatore M, Groenen R, Van Hege K and van de Sanden M C M 2008 A hard graphitelike hydrogenated amorphous carbon grown at high deposition rate (>15 nm/s) *Appl. Phys. Lett.* **92** 221502

[11] Louis E, Voorma H J, Koster N B, Shmaenok L, Bijkerk F, Schlatmann R, Verhoeven J, Platonov Y Y, Vandorssen G E and Padmore H A 1994 Enhancement of reflectivity of multilayer mirrors for soft-x-ray projection lithography by temperature optimization and ion-bombardment *Microelectron. Eng.* **23** 215–8

[12] Weber J W, Hansen T A R, van de Sanden M C M and Engeln R 2009 B-spline parametrization of the dielectric function applied to spectroscopic ellipsometry on amorphous carbon *J. Appl. Phys.* **106** 123503

[13] Tompkins H G and Irene E A (ed) 2005 *Handbook of Ellipsometry* (Norwich, NY: William Andrew Publishing/Noyes)

[14] Ferrari A C, Libassi A, Tanner B K, Stolojan V, Yuan J, Brown L M, Rodil S E, Kleinsorge B and Robertson J 2000 Density, sp(3) fraction, and cross-sectional structure of amorphous carbon films determined by x-ray reflectivity and electron energy-loss spectroscopy *Phys. Rev.* B **62** 11089–103

[15] Windt D L 1998 IMD—software for modeling the optical properties of multilayer films *Comput. Phys.* **12** 360–70

[16] Attwood D 1999 *Soft X-Rays and Extreme Ultraviolet Radiation: Principles and Applications* (Cambridge: Cambridge University Press)

[17] Kwark Y J, Bravo-Vasquez J P, Chandhok M, Cao H D, Deng H, Gullikson E and Ober C K 2006 Absorbance measurement of polymers at extreme ultraviolet wavelength: correlation between experimental and theoretical calculations *J. Vac. Sci. Technol.* B **24** 1822–6

[18] Franta D, Necas D, Zajickova L and Bursikova V 2009 Limitations and possible improvements of DLC dielectric response model based on parameterization of density of states *Diam. Relat. Mater.* **18** 413–8

[19] Franta D, Necas D, Zajickova L, Bursikova V and Cobet C 2010 Band structure of diamond-like carbon films assessed from optical measurements in wide spectral range *Diam. Relat. Mater.* **19** 114–22

[20] Zaharia T, Groenen R, Persoone P and van de Sanden M C M 2009 Graphite-like hydrogenated amorphous carbon for tribological applications grown by a remote plasma *M2i Annual Conf. (Noordwijkerhout, The Netherlands)*

[21] Chhowalla M, Robertson J, Chen C W, Silva S R P, Davis C A, Amaratunga G A J and Milne W I 1997 Influence of ion energy and substrate temperature on the optical and electronic properties of tetrahedral amorphous carbon (ta-C) films *J. Appl. Phys.* **81** 139–45

[22] Weber J W 2009 Spectroscopic ellipsometry on hydrocarbon erosion by plasma jets *Thesis* Department of Applied Physics, Eindhoven University of Technology p 78

[23] Singh S V, Zaharia T, Creatore M, Groenen R, Hege K V and van de Sanden M C M 2010 Hard graphite-like hydrogenated amorphous carbon grown at high rates by a remote plasma *J. Appl. Phys.* **107** 013305

[24] Kassavetis S, Patsalas P, Logothetidis S, Robertson J and Kennou S 2007 Dispersion relations and optical properties of amorphous carbons *Diam. Relat. Mater.* **16** 1813–22

[25] Haage T, Schmidt U I, Fath H, Hess P, Schroder B and Oechsner H 1994 Density of glow-discharge amorphous-silicon films determined by spectroscopic ellipsometry *J. Appl. Phys.* **76** 4894–6

[26] Palik E D (ed) 1985 *Handbook of Optical Constants of Solids* (San Diego, CA: Academic)

[27] Ingram D C, Woollam J A and Buabbud G 1986 Mass density and hydrogen concentration in diamond-like carbon-films—proton recoil, Rutherford backscattering and ellipsometric analysis *Thin Solid Films* **137** 225–30

[28] Graphite/HOPG 2010 http://www.nanophoenix.com/index1.html

[29] Palik E D (ed) 1991 *Handbook of Optical Constants of Solids II* (San Diego, CA: Academic)

[30] Blanco J R, Mcmarr P J, Yehoda J E, Vedam K and Messier R 1986 Density of amorphous-germanium films by spectroscopic ellipsometry *J. Vac. Sci. Technol.* A **4** 577–82

[31] Buiu O, Davey W, Lu Y, Mitrovic I Z and Hall S 2008 Ellipsometric analysis of mixed metal oxides thin films *Thin Solid Films* **517** 453–5

[32] Davey W, Buiu O, Werner M, Mitrovic I Z, Hall S and Chalker P 2009 Estimate of dielectric density using spectroscopic ellipsometry *Microelectron. Eng.* **86** 1905–7

[33] Stroud D 1998 The effective medium approximations: some recent developments *Superlattices Microstruct.* **23** 567–73

[34] Sangwal K and Kucharczyk W 1987 Relationship between density and refractive-index of inorganic solids *J. Phys. D: Appl. Phys.* **20** 522–5

[35] Nicholson D 1987 Graphite polarizability *Surf. Sci.* **181** L189–92

[36] Phillips J C 1968 Dielectric definition of electronegativity *Phys. Rev. Lett.* **20** 550–3

[37] Lide D R (ed) 2009–2010 *CRC Handbook of Chemistry and Physics* (Cambridge: Cambridge University Press)

[38] Torrens F 2001 Molecular polarizability of Sc and C (fullerene and graphite) clusters *Molecules* **6** 496–509